

Bootstrap Your Own Views: Masked Ego-Exo Modeling for Fine-grained View-invariant Video Representations

Jungin Park¹

Jiyoung Lee^{2,3*}

Kwanghoon Sohn^{1,4*}

¹Yonsei University

²Ewha Womans University

³NAVER AI Lab

⁴Korea Institute of Science and Technology (KIST)

{newrun, khsohn}@yonsei.ac.kr

lee.jiyoung@ewha.ac.kr

Abstract

View-invariant representation learning from egocentric (first-person, ego) and exocentric (third-person, exo) videos is a promising approach toward generalizing video understanding systems across multiple viewpoints. However, this area has been underexplored due to the substantial differences in perspective, motion patterns, and context between ego and exo views. In this paper, we propose a novel masked ego-exo modeling that promotes both causal temporal dynamics and cross-view alignment, called *Bootstrap Your Own Views (BYOV)*, for fine-grained view-invariant video representation learning from unpaired ego-exo videos. We highlight the importance of capturing the compositional nature of human actions as a basis for robust cross-view understanding. Specifically, self-view masking and cross-view masking predictions are designed to learn view-invariant and powerful representations concurrently. Experimental results demonstrate that our *BYOV* significantly surpasses existing approaches with notable gains across all metrics in four downstream ego-exo video tasks. The code is available at <https://github.com/park-jungin/byov>.

1. Introduction

When babies observe the actions of others – such as parents, siblings, or caregivers –, they try to replicate those actions from their own perspective. It is a fundamental capability of the human cognitive system [39, 41], known as *observational learning*. This learning arises from the recognition of natural action changes from an exocentric (*i.e.*, third-person, shortly exo) perspective to an egocentric (*i.e.*, first-person, shortly ego) perspective. The skill to recog-

* Corresponding authors.

This work was partly supported by the National Research Foundation of Korea (NRF) grant funded by the Korea government (MSIT) (No. RS-2025-00515741) and the Yonsei Signature Research Cluster Program of 2024 (2024-22-0161).

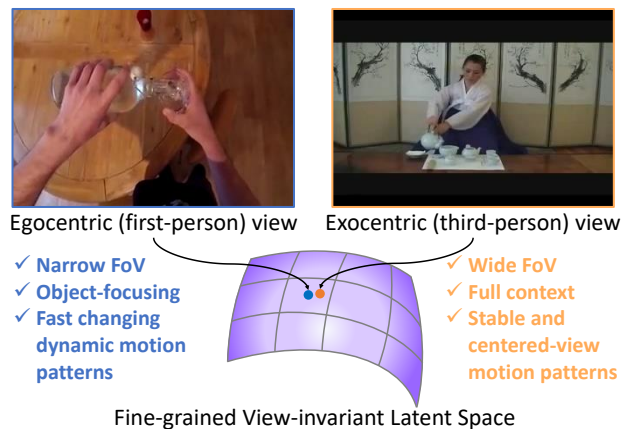


Figure 1. Challenges for view-invariant video representation learning from unpaired ego and exo videos. There is a fundamental gap between ego-exo views, such as perspective differences following the camera angle, context cues, scale and depth variations, and different motion patterns even when doing the activity.

nize the same action across different viewpoints is a crucial requirement in practice applications including robotics and augmented reality. For instance, it allows robots to understand human actions from various angles, and enables better human-robot interaction.

However, learning view-invariant representations from both ego and exo videos poses significant challenges for the following reasons; 1) The action videos taken simultaneously with ego-exo views are hard to control and collect, often impractical in real-world settings. Therefore, we might use unpaired ego-exo videos for flexible data collection. 2) There are fundamental differences in ego-exo videos in field-of-view (FoV) and scale variations, different focal points and motion patterns, and context about the environment, as illustrated in Fig. 1. In ego views, objects or actions occur closer to the camera, views are dynamically changing, and the subject often focuses on what they are directly interacting with. However, exo views are typ-

ically more stable in moving, capturing the scene from an outside angle to contain the overall background. To address those challenges, prior work [29] leveraged unpaired ego-exo video data for training, where videos are annotated with the same action class but lack temporal alignment. However, it is limited to learning clip-level coarse representations, which constrains the ability to understand sophisticated fine-grained actions in cross-view videos. Recent methods [51, 54] have demonstrated promising progress by utilizing additional hand-object interaction detectors [54] or manually crafted text annotations for specific actions [51]. It restricts the scalability, especially for diverse action classes.

In this paper, we introduce a novel method, termed as *Bootstrap Your Own Views (BYOV)*, for fine-grained view-invariant video representation learning. We argue that comprehension of the accommodation of the inherent compositionality of human actions is an essential point for learning fine-grained and view-invariant representations from unpaired ego-exo videos. To achieve this goal, we propose masked ego-exo modeling in which the model learns temporal dynamics and aligns representations across view discrepancies. First, a self-view masking prediction strategy is employed by predicting masked frame embeddings based on past embeddings in each view, capturing the temporal dependencies of fine-grained actions and events. In addition, we propose a cross-view masking strategy, where a large proportion of embeddings is masked in one view, while the visible embeddings from the other view are used to predict the masked ones. This encourages the learning of consistent representations despite variations across views.

We evaluate the robustness of **BYOV** in ego-exo benchmark [54] for four downstream fine-grained action tasks: action phase classification, frame retrieval, phase progression, and Kendall’s τ for temporal alignment. Surprisingly, our **BYOV** demonstrates significantly superior performance, outperforming existing methods by a large margin. In particular, our approach shows a remarkable improvement compared to the previous SoTA [54]. While we achieve a performance boost of over 10% in classification, our method outperforms with a margin of 3.78 mAP@10 for frame retrieval, and a margin of 0.3424 in phase progression. Additionally, in terms of Kendall’s Tau, our method demonstrates a significant gap of 0.3135, further proving its superiority across various evaluation metrics. These results highlight the effectiveness and robustness of the representations from our **BYOV** in diverse tasks.

The contributions are summarized as follows:

- We introduce a novel approach, Bootstrap Your Own Views (**BYOV**), to learn fine-grained and consistent representations from unpaired and asynchronous ego-exo videos.
- **BYOV** builds on a masked ego-exo modeling that enables

the model to learn both causal temporal dynamics and cross-view alignment.

- **BYOV** achieves SoTA performance by a significant margin across several downstream tasks, demonstrating the superiority of our learned representations.

2. Related Work

Fine-grained action recognition has gained significant attention in distinguishing between subtle variations in actions that often involve similar movements or interactions. Previous works for exocentric video understanding have recognized fine-grained actions by compositions of components, using the combinations of sub-actions [30, 36], words with language knowledge [12, 23, 34], or specified attributes [40, 56, 57]. Otherwise, EPIC-Kitchens [8] and Ego4D [16] have been released as valuable benchmarks in egocentric activity understanding. Ego models for fine-grained action recognition have relied on temporal aggregation with global frame features [25, 31, 38] or hand-object interactions [24, 32, 48]. However, those approaches trained on ego videos are limited in handling extreme variations in viewpoints. To tackle this problem, view-invariant learning [1, 55] has explored recognizing action in both ego and exo videos, but they require simultaneously captured ego-exo videos [17]. Meanwhile, Ego-Exo [29] and AE2 [54], which are highly related to our work, have been proposed for reliable representation learning from unpaired ego-exo videos. Although Ego-Exo [29] has introduced a promising exo-to-ego transfer learning framework, it relies on the pretrained models [14] to augment pseudo labels. The most recent work is AE2 [54], introducing a new benchmark for fine-grained cross-view activity understanding. However, an ego-exo temporal alignment framework proposed in AE2 heavily relies on off-the-shelf hand-object interaction detectors [44] with a classical alignment objective, *i.e.* dynamic time warping (DTW) [3], which limits to computing the optimal alignment between unpaired different view videos.

Masked modeling in videos, inspired by the success of masked language models such as BERT [10], has recently shown promise for learning rich spatiotemporal representations from videos in a self-supervised manner. Commonly, a transformer-based encoder-decoder architecture [21] is used to reconstruct masked portions of frame sequences. The encoder captures contextual information to infer missing content in the decoder. For instance, VideoMAE [49] employs masked autoencoding by making video patches across both temporal and spatial views. Instead, MaskFeat [53] performs the masked modeling to directly regress the features (*e.g.*, HOG [7]). Meanwhile, some works [2, 18] have used a discrete variational autoencoder (dVAE) to compress frames into smaller visual tokens. Contrary to the works for exocentric video [15, 47, 49, 53], masked

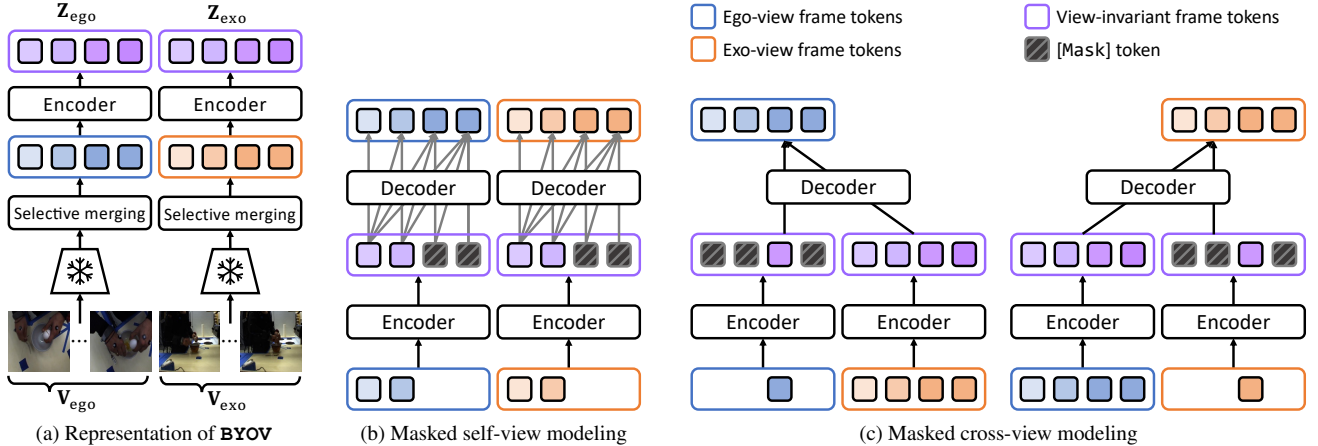


Figure 2. The overall framework of **BYOV**. The proposed masked (b) self-view and (c) cross-view modeling encourages learning fine-grained view-invariant representations from unpaired ego and exo videos. We employ an encoder-decoder framework across disparate views, which is trained simultaneously to predict both frame tokens from its own view and frame tokens from a different view performing the same action. As shown in (a), we note that the decoder is discarded in performing downstream tasks.

modeling has also been explored to learn egocentric video representations in a data-efficient manner [50]. While the method has shown strong transferability across egocentric video tasks, such as action recognition and robot manipulation, it has only been applied to single-view ego videos. As a result, the effectiveness of masked modeling for cross-view video representation learning remains largely unexplored.

3. Bootstrap Your Own Views

3.1. Overview of BYOV

Given unpaired and asynchronous ego and exo videos (*i.e.*, recorded independently, but belonging to the same action class), our primary goal is to learn the temporal dependency of sophisticated action and view invariance features. To this end, we incorporate robust masked visual modeling [21] into fine-grained view-invariant video representation learning. In contrast to previous works [21, 49] that predict masked patches in self-supervision only, our **BYOV** employs two different masked modeling methods according to the learning objects. First, masked self-view modeling reconstructs frame-level token embeddings from the own view video to capture the temporal dependency of fine-grained activity between dense frames. Secondly, masked cross-view modeling learns view-invariant temporal features by predicting the different view’s latents from one another.

BYOV consists of three modules: 1) a pre-trained image encoder to extract frame token embeddings; 2) a transformer encoder to map frame embeddings to a view-invariant latent space; and 3) a transformer decoder to reconstruct masked frame embeddings. Specifically, vision transformers [11, 33] compute patch-wise features for each

frame, but it increases the computation demands to process all frames in the video. Given that frames in the video containing fine-grained activity are slightly different in spatial regions, we introduce a frame token embedding selection approach to efficiently estimate global frame token embeddings. For the transformer-based encoder and decoder, we adopt an asymmetric design following the previous works [21, 49] where the encoder processes only the partial frame token embeddings, while the decoder reconstructs the whole frame token embeddings from the view-invariant embeddings and mask token embeddings. After pretraining, the decoder is discarded and the encoder is used to project each frame from ego and exo videos into the shared view-invariant latent space. In the following sections, we present **BYOV** in detail.

3.2. Frame encoding

Let $f_{\theta}(\cdot)$ represent an image encoder (*e.g.*, ViT [11]) pre-trained from image datasets, parameterized by θ , $\mathbf{V}_{ego} = \{\mathbf{v}_{ego}^t\}_{t=1}^{T_{ego}}$ and $\mathbf{V}_{exo} = \{\mathbf{v}_{exo}^t\}_{t=1}^{T_{exo}}$ are an ego and exo video composing sequence of T_{ego} and T_{exo} frames, respectively. For each view video, we first encode frames with $f_{\theta}(\cdot)$ into d -dimensional embedding space to obtain N token embeddings for each frame, such that,

$$\begin{aligned} \mathbf{X}_{ego} &= \{\mathbf{x}_{ego}^t\}_{t=1}^{T_{ego}} = f_{\theta}(\mathbf{V}_{ego}) \in \mathbb{R}^{T_{ego} \times N \times d}, \\ \mathbf{X}_{exo} &= \{\mathbf{x}_{exo}^t\}_{t=1}^{T_{exo}} = f_{\theta}(\mathbf{V}_{exo}) \in \mathbb{R}^{T_{exo} \times N \times d}. \end{aligned} \quad (1)$$

To reduce the training cost, we keep the image encoder frozen during training. Even though image embeddings from the pretrained image encoder have robust representative power, they are often limited to capturing temporal dynamics [35]. We thereby develop **BYOV** to use those embeddings in the ego-exo representation learning with videos.

3.3. Selective token merging

Typically views representing atomic human actions are visually similar, and show only slight local differences (typically around a hand-object interaction region) across frames. For this reason, fine-grained representations have to be captured in ego-exo videos. While AE2 [54] has employed hand-object interaction detector [44] to capture action-related regions, some ego works [22, 37] have incorporated additional temporal dynamic signals such as optical flows and eye gaze signals. However, they have increased the burden of computational costs.

Instead, we propose a simple but effective alternative solution that selects a set of tokens based on the difference between token embeddings of consecutive frames. Since local patches of each frame are encoded into each token embedding in the vision transformer, the difference between token embeddings located in the same position but from different frames can naively reflect the transition of local regions over time [5]. Specifically, we compute the absolute difference value of the token embeddings between two consecutive frames and select top- K tokens with large values:

$$n^t = \arg \text{top-K}(\mathbf{s}^t),$$

$$\text{where } \mathbf{s}^t = \frac{1}{d} \sum_d |\mathbf{x}^t - \mathbf{x}^{t+1}| \in \mathbb{R}^N, \quad (2)$$

where n^t indicates the indices of the selected tokens in each frame. The selected K token embeddings are averaged to obtain a set of frame token embeddings $\bar{\mathbf{X}}_{\text{ego}} \in \mathbb{R}^{T_{\text{ego}} \times d}$ and $\bar{\mathbf{X}}_{\text{exo}} \in \mathbb{R}^{T_{\text{exo}} \times d}$, which are used as the masked-target and encoded token embeddings to be reconstructed by the encoder $g_\phi(\cdot)$ and the decoder $h_\psi(\cdot)$.

3.4. Masked self-view modeling (MSM)

To learn the temporal dependency for fine-grained action recognition, we propose masked self-view modeling (MSM). We randomly sample a subset of frame tokens and remove the remaining ones. The sampled frame token embeddings from each view, $\bar{\mathbf{X}}_{\text{ego}}^{\text{MSM}}$ and $\bar{\mathbf{X}}_{\text{exo}}^{\text{MSM}}$, are respectively mapped to the latent space that is used as a shared view-invariant embedding space, through the encoder $g_\phi(\cdot)$:

$$\mathbf{Z}_{\text{ego}}^{\text{MSM}} = g_\phi(\bar{\mathbf{X}}_{\text{ego}}^{\text{MSM}}) \in \mathbb{R}^{T_{\text{ego}}^{\text{MSM}} \times d},$$

$$\mathbf{Z}_{\text{exo}}^{\text{MSM}} = g_\phi(\bar{\mathbf{X}}_{\text{exo}}^{\text{MSM}}) \in \mathbb{R}^{T_{\text{exo}}^{\text{MSM}} \times d}. \quad (3)$$

The decoder $h_\psi(\cdot)$ reconstructs the original frame token embeddings (*i.e.*, $\bar{\mathbf{X}}_{\text{ego}}$ and $\bar{\mathbf{X}}_{\text{exo}}$) from the full set of frame tokens, consisting of frame tokens from the encoder (*i.e.*, \mathbf{Z}'_{ego} and \mathbf{Z}'_{exo}) and learnable mask tokens [10] filled into the position of removed tokens. We refer to this full set of frame tokens as ‘‘mask-filled tokens’’. We add positional embeddings to all tokens to enable the decoder to take the dependency over time into account. To guarantee temporal dependency for mask prediction, we apply a causal mask [10]

to attention layers in the decoder so that the decoder reconstructs the t -th frame token only from the previous $(t - 1)$ tokens.

The objective of MSM is defined by the mean squared error (MSE) between the reconstructed and original frame token embeddings:

$$\mathcal{L}_{\text{MSM}} = \frac{1}{T_{\text{ego}}} \|\bar{\mathbf{X}}_{\text{ego}} - \mathbf{Y}_{\text{ego}}^{\text{MSM}}\|_2 + \frac{1}{T_{\text{exo}}} \|\bar{\mathbf{X}}_{\text{exo}} - \mathbf{Y}_{\text{exo}}^{\text{MSM}}\|_2,$$

$$\text{where } \mathbf{Y}_{\text{ego}}^{\text{MSM}} = h_\psi(\mathbf{Z}'_{\text{ego}} \parallel [\text{mask}]),$$

$$\mathbf{Y}_{\text{exo}}^{\text{MSM}} = h_\psi(\mathbf{Z}'_{\text{exo}} \parallel [\text{mask}]). \quad (4)$$

We highlight that masking prediction is performed at the frame feature level, not the original frame image reconstruction. It can significantly reduce the computational training cost for the autoencoding process [52]. Furthermore, it preserves strong spatial representation from the image encoder, while the encoder concentrates on learning temporal context with visual cues. Fig. 2b illustrates the overall process of the MSM.

3.5. Masked cross-view modeling (MCM)

While MSM enables the model to capture the temporal dependency between frames within the same view video, masked cross-view modeling (MCM) aims to learn the view-invariant alignment between the different view videos. Similar to MSM, we first project the whole frame tokens (*i.e.*, $\bar{\mathbf{X}}_{\text{ego}}$ and $\bar{\mathbf{X}}_{\text{exo}}$) into the latent space, such that,

$$\mathbf{Z}_{\text{ego}} = g_\phi(\bar{\mathbf{X}}_{\text{ego}}), \quad \mathbf{Z}_{\text{exo}} = g_\phi(\bar{\mathbf{X}}_{\text{exo}}). \quad (5)$$

Concurrently, we randomly remove a subset of frame tokens with a larger ratio than in MSM, and map to the latent space (see Fig. 2c):

$$\mathbf{Z}_{\text{ego}}^{\text{MCM}} = g_\phi(\bar{\mathbf{X}}_{\text{ego}}^{\text{MCM}}) \in \mathbb{R}^{T_{\text{ego}}^{\text{MCM}} \times d},$$

$$\mathbf{Z}_{\text{exo}}^{\text{MCM}} = g_\phi(\bar{\mathbf{X}}_{\text{exo}}^{\text{MCM}}) \in \mathbb{R}^{T_{\text{exo}}^{\text{MCM}} \times d}, \quad (6)$$

where $\bar{\mathbf{X}}_{\text{ego}}^{\text{MCM}}$ and $\bar{\mathbf{X}}_{\text{exo}}^{\text{MCM}}$ are remaining frame tokens after masking. We note that the number of retention frames varies between ego and exo videos. In MCM, the decoder reconstructs the original frame token embeddings of one view video from the mask-filled tokens of its own view and the latents of another view:

$$\mathbf{Y}_{\text{ego}}^{\text{MCM}} = h_\psi(\mathbf{Z}_{\text{ego}}^{\text{MCM}} \parallel [\text{mask}] \parallel \mathbf{Z}_{\text{exo}}),$$

$$\mathbf{Y}_{\text{exo}}^{\text{MCM}} = h_\psi(\mathbf{Z}_{\text{exo}}^{\text{MCM}} \parallel [\text{mask}] \parallel \mathbf{Z}_{\text{ego}}). \quad (7)$$

The objective of MCM can be formulated by the MSE between the reconstructed and original frame token embeddings:

$$\mathcal{L}_{\text{MCM}} = \frac{1}{T_{\text{ego}}} \|\bar{\mathbf{X}}_{\text{ego}} - \mathbf{Y}_{\text{ego}}^{\text{MCM}}\|_2 + \frac{1}{T_{\text{exo}}} \|\bar{\mathbf{X}}_{\text{exo}} - \mathbf{Y}_{\text{exo}}^{\text{MCM}}\|_2. \quad (8)$$

We force the cross-view generation as $\mathbf{Z}_{\text{ego}}^{\text{MCM}}$ and $\mathbf{Z}_{\text{exo}}^{\text{MCM}}$ contain only a small subset (e.g. 20% in MCM vs. 60 % in MSM) of the full tokens. Namely, the decoder is forced to reconstruct the original frame tokens from another view’s tokens. This allows us to learn view-invariant latent space.

3.6. Joint training with MSM and MCM

The final objective of **BYOV** is the sum of the objectives of MSM and MCM:

$$\mathcal{L}_{\text{BYOV}} = \mathcal{L}_{\text{MSM}} + \mathcal{L}_{\text{MCM}}. \quad (9)$$

While both loss terms serve a similar purpose (i.e., masked token embedding reconstruction), they operate differently based on the varying inputs to the decoder. The joint training aims to achieve both objectives simultaneously by enabling the encoder to map view-invariant features from ego-exo videos into a shared latent space. We notice that the forward-backward pass is separately performed by the loss, but the framework shares the same parameters.

4. Experiments

4.1. Evaluation setup

The essential capabilities of fine-grained, view-invariant video representations are 1) fine-grained temporal understanding of the given action and 2) alignment across cross-view videos. Following previous work [54], we evaluate **BYOV** on four datasets in the ego-exo benchmark [54], including *Break Eggs*, *Pour Milk*, *Pour Liquid*, and *Tennis Forehand*. Each dataset consists of four tasks as follows:

- **Action phase classification** aims to predict an atomic action phase label corresponding to a given frame. For example, ‘Break Eggs’ dataset contains four action phases following the key events, such as ‘hit egg’, ‘visible crack on the eggshell’, ‘egg contents released into bowl.’ Following [54], we train an SVM classifier with the embeddings from the training set and evaluate the F1 score on the test set. We evaluate the performance in two settings: the regular setting, where the classifier is trained using embeddings from both views, and the cross-view setting, where training and testing data are sourced from different view videos.
- **Frame retrieval** shares the same context with classification in evaluation, but does not require additional training. We evaluate the performance with Nearest Neighbor search (NN) to retrieve frames and report mean average precision (mAP)@10 performance in the regular and cross-view settings.
- **Phase progression** evaluates how accurately the embeddings capture the progress of an action over time by predicting the phase progression values defined as the timestamp difference between each frame and key events, normalized by the total number of frames in the video [13].

We train a linear regressor with the embeddings and evaluate the average R-square.

- **Kendall’s τ** measures how well-aligned two given sequences are in time. We first sample a pair of frames in one video and retrieve the corresponding nearest frames from another video. Kendall’s τ measures concordant, which represents whether the order of the retrieved frame pair matches the order of the frame pair in the first video, over every pair of frames in a pair of videos.

Each dataset contains a varying number of subjects, and each subject is captured from different equipment. A detailed description of the evaluation benchmark is demonstrated in Appendix A.

In addition, we evaluate video-level action recognition performance on the Charades-Ego dataset [46], which contains 4k paired ego-exo videos, using the linear probing protocol. Specifically, our model is trained on the Charades-Ego training set, and video-level embeddings are averaged by frame-level embeddings. We train a linear classifier with video embeddings and report mAP scores on the test set.

4.2. Implementation details

We employ CLIP pretrained ViT-B/16 [11] as the image encoder $f_{\theta}(\cdot)$, and freeze it. We take the last hidden states of the image encoder except for a class token. The encoder and decoder for masked modeling have 12 and 4 Transformer blocks, respectively, with 256-dimensional embedding space. We learn frame embedding encoder $g_{\phi}(\cdot)$ and the decoder $h_{\psi}(\cdot)$ on the training set, while $g_{\phi}(\cdot)$ is frozen during the training of SVM classifier and the linear regression for evaluation. The decoder is discarded after training. Note that the encoder and decoder have only 9.7M and 2.6M parameters respectively. We empirically set the token selection ratio to 0.3 and the masking ratio in the self-view prediction and cross-view prediction to 0.4 and 0.8, respectively. For the Break Eggs, Pour Milk, and Pour Liquid datasets, we randomly sample 32 frames to cover the whole video for training and use all frames for evaluation. For the Tennis Forehand dataset, we use randomly sampled 20 frames for training as they have shorter video lengths. For Charades-Ego, we randomly sample 32 frames for training. While ego-exo videos are synchronized, we do not use the temporal correspondence between videos for training.

Baselines. We compare the performance of **BYOV** against a variety of baselines with different characteristics: (1) Randomly initialized feature (**Random features**), **ImageNet features** from the ResNet-50 [20] pretrained on ImageNet [9], and **CLIP features** from the CLIP ViT-B/16 pretrained on LAION-400M [42] which is used as the frame feature in **BYOV**. (2) Self-supervised view-invariant video representation learning (**TCN [43]**, **ActorObserverNet [45]**). (3) Fine-grained video representation learning (**CARL [4]**, **TCC [13]**, **GTA [19]**). (4) Fine-grained view-

Table 1. Performance comparison with the state-of-the-art methods [4, 19, 43, 45, 54] on the AE2 benchmark [54]. The benchmark consists of four sub-tasks: (A) Break Eggs, (B) Pour Milk, (C) Pour Liquid, and (D) Tennis Forehand.

Task	Method	Classification (F1 score)			Frame Retrieval (mAP@10)			Phase progression	Kendall's τ
		Regular	Ego2Exo	Exo2Ego	Regular	Ego2Exo	Exo2Ego		
(A)	Random features	19.18	18.93	19.45	47.13	41.74	37.19	-0.0572	0.0018
	ImageNet features	50.24	21.48	32.25	50.49	33.09	37.80	-0.1446	0.0188
	CLIP features	51.66	27.97	26.24	44.46	35.85	35.70	0.0402	0.0168
	ActorObserverNet [45]	36.14	36.40	31.00	50.47	42.70	41.29	-0.0517	0.0024
	TCN [43] (single-view)	56.90	18.60	35.61	53.42	32.63	34.91	0.0051	0.1206
	TCN [43] (multi-view)	59.91	48.65	56.91	58.83	47.04	52.68	0.2669	0.2886
	CARL [4]	43.43	28.35	29.22	46.04	37.38	39.94	-0.0837	-0.0091
	TCC [13]	59.84	54.17	52.28	58.75	61.11	62.03	0.2880	0.5191
	GTA [19]	56.86	52.33	58.35	61.55	56.25	53.93	0.3462	0.4626
	AE2 [54]	66.23	57.41	71.72	65.85	64.59	62.15	0.5109	0.6316
BYOV	74.30	75.01	71.28	67.17	70.65	69.02	0.8533	0.9451	
(B)	Random features	36.84	33.96	41.97	52.48	50.56	51.98	-0.0477	0.0050
	ImageNet features	41.59	39.93	45.52	54.09	27.31	43.21	-2.6681	0.0115
	CLIP features	43.24	49.21	30.94	52.16	46.39	40.34	-4.0754	0.0046
	TCN [43] (single-view)	47.39	43.44	42.28	57.00	46.48	47.20	-0.3238	-0.0197
	CARL [4]	48.79	52.41	43.01	55.01	52.99	51.51	-0.1639	0.0443
	TCC [13]	77.91	72.29	81.07	80.97	75.30	80.27	0.6665	0.7614
	GTA [19]	81.11	74.94	81.51	80.12	72.78	75.40	0.7086	0.8022
	AE2 [54]	85.17	84.73	82.77	84.90	78.48	83.41	0.7634	0.9062
BYOV	86.46	85.09	86.61	89.42	87.73	85.06	0.8992	0.9466	
(C)	Random features	45.26	47.45	44.33	49.83	55.44	55.75	-0.1303	-0.0072
	ImageNet features	53.13	22.44	44.61	51.49	52.17	30.44	-1.6329	-0.0053
	CLIP features	60.60	36.97	48.43	43.63	47.58	37.02	-0.3139	-0.0048
	TCN [43] (single-view)	54.02	32.77	51.24	48.83	55.28	31.15	-0.5283	0.0103
	CARL [4]	56.98	47.46	52.68	55.29	59.37	36.80	-0.1176	0.0085
	TCC [13]	52.53	43.85	42.86	62.33	56.08	57.89	0.1163	0.1103
	GTA [19]	56.92	42.97	59.96	62.79	58.52	53.32	-0.2370	0.1005
	AE2 [54]	66.56	57.15	65.60	65.54	65.79	57.35	0.1380	0.0934
BYOV	79.48	71.83	76.23	71.06	75.03	70.03	0.4483	0.3052	
(D)	Random Features	30.31	33.42	28.10	66.47	58.98	59.87	-0.0425	0.0177
	ImageNet Features	69.15	42.03	58.61	76.96	66.90	60.31	-0.4143	0.0734
	CLIP Features	67.81	43.41	44.22	74.54	59.57	52.02	-0.4996	0.0618
	TCN [43] (single-view)	68.87	48.86	36.48	73.76	55.08	56.65	-0.0602	0.0737
	CARL [4]	59.69	35.19	47.83	69.43	54.83	63.19	-0.1310	0.0542
	TCC [13]	78.41	53.29	32.87	80.24	55.84	63.19	0.2155	0.1040
	GTA [19]	83.63	82.91	81.80	85.20	78.00	79.14	0.4691	0.4901
	AE2 [54]	85.87	84.71	85.68	86.83	81.46	82.07	0.5060	0.6171
BYOV	89.12	94.47	85.73	90.61	88.34	88.94	0.7881	0.7852	

invariant video representation learning (AE2 [54]) that is directly comparable to our **BYOV**.

4.3. Results

Quantitative comparisons on AE2. In Tab. 1, we present the performance of each task across four ego-exo datasets. The comparison between ImageNet and CLIP features reveals that the differences between the encoder architecture

(*i.e.*, CNNs [20] vs. transformers [11]), and the scale of the pretraining dataset (*i.e.*, 1.3M [9] vs. 400M [42]) have minimal impact on fine-grained, view-invariant video understanding. Notably, both features struggle to capture the progress of an action over time especially in the cross-view. Consequently, they show poor performance in phase progression and Kendall's τ tasks even than random features. Meanwhile, **BYOV** significantly outperforms exist-

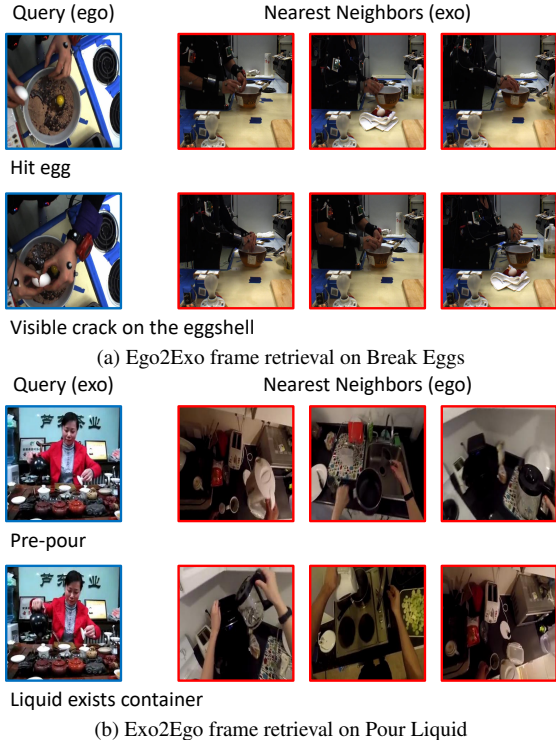


Figure 3. Results of frame retrieval from *Break Eggs* and *Pour Liquid*. We retrieve the nearest neighbor frames (red box) corresponding to the given query frame (blue box).

ing SoTAs [19, 54]. The comparison between baselines and **BYOV** demonstrates the powerful representative capability of **BYOV**. Especially, our **BYOV** outperforms others in in-the-wild scenarios as shown in the ‘Pour Liquid’ and ‘Tennis Forehand’ datasets. It illustrates that our masked modeling is more effective self-supervision than previous works [43, 45] for real-world videos. In Appendix B, we provide additional results with CLIP pretrained ViT-L/14 [11], and also provide the F1 scores for few-shot classification, mAP@5, and mAP@15 for frame retrieval.

Qualitative results on AE2. In Fig. 3, we depict examples for cross-view frame retrieval from the *Break Eggs* and *Pour Liquid* datasets. We retrieve the frames (red box) in all test frames from the query frame (blue box) using NN search. The query frame and retrieved frames are obtained from different views. The results show that the query and retrieved frames are contextually connected through the action state despite the significant visual discrepancy between the ego-exo views. In Fig. 3a, for example, egocentric representations from **BYOV** successfully distinguish ‘hit egg’ and ‘visible crack on the eggshell’ phases to retrieve corresponding frames in exocentric videos. More qualitative results are illustrated in Appendix B.3.

tSNE visualization on AE2. Fig. 4 illustrates tSNE visualization of frame embeddings (a) before training and (b)

Table 2. Performance comparison on Charades-Ego.

Method	Regular	Ego2Ego	Exo2Ego
Random features	7.2	7.1	7.2
CLIP features (ViT-B/16)	13.7	8.3	10.7
BYOV (ViT-B/16)	31.8	26.5	27.3

Table 3. Performance with respect to variants of the components in **BYOV**. We report the performance evaluated on *Break Eggs*.

Method	F1 score	mAP@10	Progr.	τ
BYOV	73.53	68.95	0.8533	0.9451
– Token selection	71.84	67.55	0.8224	0.9016
– Causal mask	72.29	68.10	0.6420	0.7091
– MSM	62.12	60.34	0.4362	0.4906
– MCM	57.43	55.83	0.6724	0.7086

trained with **BYOV**. We sample four videos (two ego and two exo videos) from the *Break Eggs* dataset, and distinguish views and action phases by shapes of the point (circle for ego, and square for exo) and colors, respectively. Before training, we can observe a clear gap between the frame embeddings (from the ViT-B/16) according to the viewpoint and video ID, while the embeddings clumped together regardless of the action phases, as shown in Fig. 4a. We argue that pretrained image encoders are hard to capture discriminative features for the action phase due to the large visual similarity between frames. Surprisingly, the frame representations obtained from **BYOV** form trajectories according to the action phase, regardless of the viewpoint, as shown in Fig. 4b. The result demonstrates that **BYOV** effectively learns temporal dynamics and accomplishes view invariance.

Results on Charades-Ego. We compare the performance of Random features, CLIP features from the CLIP ViT-B/16, and **BYOV** with the CLIP ViT-B/16 on Charades-Ego. We measure mAP scores using linear probing with three evaluation settings, as shown in Tab. 2: ‘Regular,’ which utilizes both ego and exo videos for training; ‘Ego2Ego,’ where the classifier is trained on ego videos and tested on exo videos; and ‘Exo2Ego,’ which performs the reverse. **BYOV** significantly improves mAP scores by 18.1%, 18.2%, and 16.6% in each setting, demonstrating its effectiveness even in the video-level action understanding.

4.4. Component analysis

Token selection. We select K tokens based on the difference between token embeddings from consecutive frames to encode the action-related spatial information. Since fine-grained action recognition requires detecting subtle yet critical movements, it is important to utilize selective features effectively without noisy redundant information. To verify

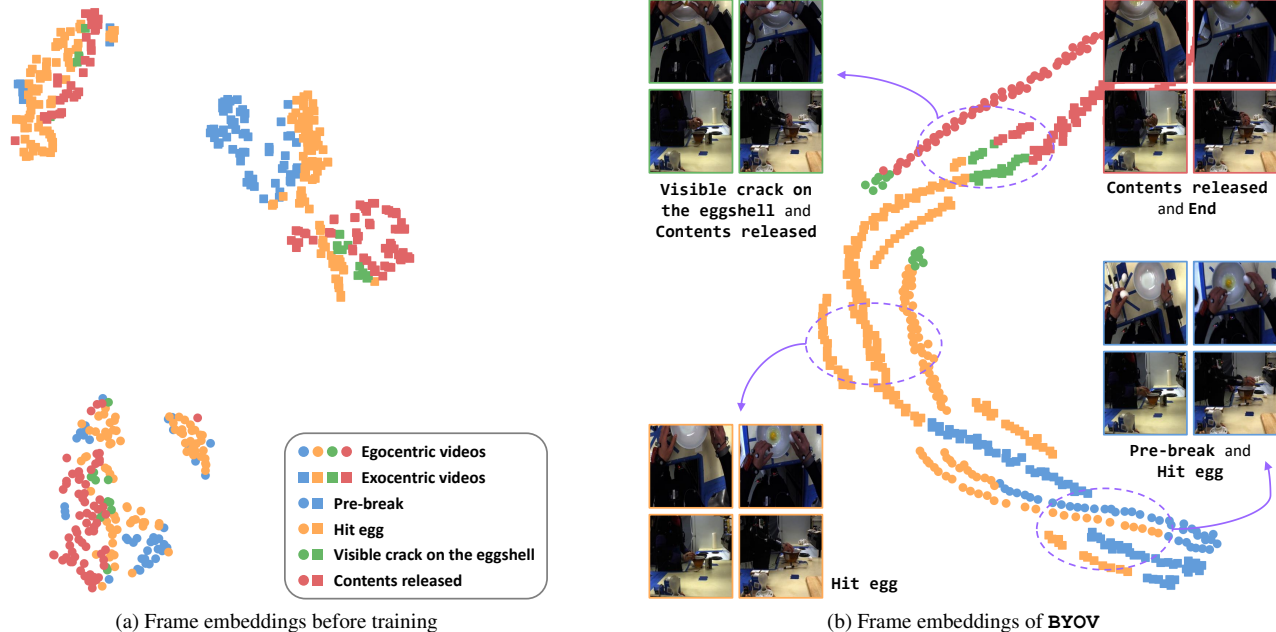


Figure 4. tSNE visualization of frame embeddings (a) before training and (b) trained with **BYOV**. We sample two ego and two exo videos from *Break Eggs*.

the effectiveness of token selection, we evaluate the performance without token selection as shown in Tab. 3 (**BYOV** –Token selection). The result shows that selective token merging improves the performance in all metrics. Ablation studies and visualization corresponding to the token selection ratio are provided in Appendix B.4.

Causal mask in MSM. We apply the causal mask in the decoder during MSM to enable the model to learn the temporal dependency between frames. Tab. 3 (**BYOV** –Causal mask) demonstrates the impact of the causal mask. Especially, the performance is notably degraded in both phase progression and Kendall’s τ , showing the significance of apprehending causality to downstream tasks.

Masked modeling. Tab. 3 demonstrates the effectiveness of the choice of masked modeling methods. **BYOV** –MSM shows that the performance significantly drops across all tasks, especially in phase progression and Kendall’s τ that are highly related to the causality between frames. The results demonstrate the effectiveness of MSM in learning the temporal dependency for fine-grained action recognition. Meanwhile, the ablation study for MCM (**BYOV** –MCM) shows significant performance drops in the cross-view classification and retrieval tasks. The results demonstrate that MCM and MSM complement each other from different perspectives. Both masked modelings enable robust view-invariant learning across egocentric and exocentric videos, thereby effects for fine-grained video understanding. We provide the effectiveness of representations corresponding to the masking ratio in MSM and MCM in Appendix B.4.

5. Conclusion

We propose **BYOV** to learn view-invariant video representations with masked ego-exo modeling. During training, our method simultaneously predicts self- and cross-view feature masking tokens in a self-supervised manner with unpaired and asynchronous egocentric and exocentric videos. While masked self-view modeling boosts the model to capture fine-grained temporal dependency in actions, masked cross-view modeling accelerates cross predictions by view-invariant video representations. Moreover, our selective token merging approach is simple, yet can be an effective alternative for off-the-shelf human-object interaction detectors or additional temporal dynamic signals, without the additional burden of computational cost. **BYOV** achieves state-of-the-art performance with significantly larger margins than existing methods for cross-view invariant learning in four downstream video tasks.

Acknowledgement. This work was supported by the Institute of Information & communications Technology Planning & Evaluation (ITP) grant funded by the Korea government (MSIT) (No. RS-2022-0015966, Artificial Intelligence Convergence Innovation Human Resources Development (Ewha Womans University)).

References

- [1] Shervin Ardeshtir and Ali Borji. An exocentric look at egocentric actions and vice versa. *CVIU*, 171:61–68, 2018. 2

- [2] Hangbo Bao, Li Dong, Songhao Piao, and Furu Wei. Beit: Bert pre-training of image transformers. In *ICLR*, 2022. 2
- [3] Donald J Berndt and James Clifford. Using dynamic time warping to find patterns in time series. In *KDD*, 1994. 2
- [4] Minghao Chen, Fangyun Wei, Chong Li, and Deng Cai. Frame-wise action representations for long videos via sequence contrastive learning. In *CVPR*, 2022. 5, 6, 13, 14, 15
- [5] Joonmyung Choi, Sanghyeok Lee, Jaewon Chu, Minhyuk Choi, and Hyunwoo J Kim. vid-tldr: Training free token merging for light-weight video transformer. In *CVPR*, 2024. 4
- [6] Rohan Choudhury, Guanglei Zhu, Sihan Liu, Koichiro Niinuma, Kris Kitani, and László Jeni. Don't look twice: Faster video transformers with run-length tokenization. In *NeurIPS*, pages 28127–28149, 2024. 18
- [7] Navneet Dalal and Bill Triggs. Histograms of oriented gradients for human detection. In *CVPR*, 2005. 2
- [8] Dima Damen, Hazel Doughty, Giovanni Maria Farinella, Sanja Fidler, Antonino Furnari, Evangelos Kazakos, Davide Moltisanti, Jonathan Munro, Toby Perrett, Will Price, et al. Scaling egocentric vision: The epic-kitchens dataset. In *ECCV*, 2018. 2, 11
- [9] Jia Deng, Wei Dong, Richard Socher, Li-Jia Li, Kai Li, and Li Fei-Fei. Imagenet: A large-scale hierarchical image database. In *CVPR*, 2009. 5, 6, 15
- [10] Jacob Devlin, Ming-Wei Chang, Kenton Lee, and Kristina Toutanova. Bert: Pre-training of deep bidirectional transformers for language understanding. In *NAACL*, 2019. 2, 4
- [11] Alexey Dosovitskiy, Lucas Beyer, Alexander Kolesnikov, Dirk Weissenborn, Xiaohua Zhai, Thomas Unterthiner, Mostafa Dehghani, Matthias Minderer, Georg Heigold, Sylvain Gelly, Jakob Uszkoreit, and Neil Houlsby. An image is worth 16x16 words: Transformers for image recognition at scale. In *ICLR*, 2021. 3, 5, 6, 7, 11
- [12] Hazel Doughty and Cees GM Snoek. How do you do it? fine-grained action understanding with pseudo-adverbs. In *CVPR*, 2022. 2
- [13] Debidatta Dwibedi, Yusuf Aytar, Jonathan Tompson, Pierre Sermanet, and Andrew Zisserman. Temporal cycle-consistency learning. In *CVPR*, 2019. 5, 6, 13, 14, 15
- [14] Christoph Feichtenhofer, Haoqi Fan, Jitendra Malik, and Kaiming He. Slowfast networks for video recognition. In *ICCV*, pages 6202–6211, 2019. 2
- [15] Christoph Feichtenhofer, Yanghao Li, Kaiming He, et al. Masked autoencoders as spatiotemporal learners. *NeurIPS*, pages 35946–35958, 2022. 2
- [16] Kristen Grauman, Andrew Westbury, Eugene Byrne, Zachary Chavis, Antonino Furnari, Rohit Girdhar, Jackson Hamburger, Hao Jiang, Miao Liu, Xingyu Liu, et al. Ego4d: Around the world in 3,000 hours of egocentric video. In *CVPR*, 2022. 2
- [17] Kristen Grauman, Andrew Westbury, Lorenzo Torresani, Kris Kitani, Jitendra Malik, Triantafyllos Afouras, Kumar Ashutosh, Vijay Baiyya, Siddhant Bansal, Bikram Boote, et al. Ego-exo4d: Understanding skilled human activity from first-and third-person perspectives. In *CVPR*, pages 19383–19400, 2024. 2
- [18] Agrim Gupta, Stephen Tian, Yunzhi Zhang, Jiajun Wu, Roberto Martín-Martín, and Li Fei-Fei. Maskvit: Masked visual pre-training for video prediction. In *ICLR*, 2023. 2
- [19] Isma Hadji, Konstantinos G. Derpanis, and Allan D. Jepson. Representation learning via global temporal alignment and cycle-consistency. In *CVPR*, 2021. 5, 6, 7, 13, 14, 15
- [20] Kaiming He, Xiangyu Zhang, Shaoqing Ren, and Jian Sun. Deep residual learning for image recognition. In *CVPR*, 2016. 5, 6, 11, 15
- [21] Kaiming He, Xinlei Chen, Saining Xie, Yanghao Li, Piotr Dollár, and Ross Girshick. Masked autoencoders are scalable vision learners. In *CVPR*, 2022. 2, 3
- [22] Yifei Huang, Guo Chen, Jilan Xu, Mingfang Zhang, Lijin Yang, Baoqi Pei, Hongjie Zhang, Lu Dong, Yali Wang, Limin Wang, and Yu Qiao. Egoexolearn: A dataset for bridging asynchronous ego- and exo-centric view of procedural activities in real world. In *CVPR*, 2024. 4
- [23] Jingwei Ji, Ranjay Krishna, Li Fei-Fei, and Juan Carlos Nieves. Action genome: Actions as compositions of spatio-temporal scene graphs. In *CVPR*, 2020. 2
- [24] Georgios Kapidis, Ronald Poppe, Elsbeth Van Dam, Lucas Noldus, and Remco Veltkamp. Egocentric hand track and object-based human action recognition. In *UIC-ATC*, 2019. 2
- [25] Evangelos Kazakos, Arsha Nagrani, Andrew Zisserman, and Dima Damen. Epic-fusion: Audio-visual temporal binding for egocentric action recognition. In *ICCV*, 2019. 2
- [26] Hildegard Kuehne, Hueihan Jhuang, Estíbaliz Garrote, Tomaso Poggio, and Thomas Serre. Hmdb: A large video database for human motion recognition. In *ICCV*, 2011. 11
- [27] Taein Kwon, Bugra Tekin, Jan Stühmer, Federica Bogo, and Marc Pollefeys. H2o: Two hands manipulating objects for first person interaction recognition. In *ICCV*, 2021. 11
- [28] Fernando De la Torre, Jessica Hodgins, Adam Bargaiteil, Xavier Martin, Justin Macey, Alex Collado, and Pep Beltran. Guide to the carnegie mellon university multimodal activity (cmu-mmact) database. *Tech. report CMU-RI-TR-08-22*, 2009. 11
- [29] Yanghao Li, Tushar Nagarajan, Bo Xiong, and Kristen Grauman. Ego-exo: Transferring visual representations from third-person to first-person videos. In *CVPR*, 2021. 2
- [30] Zhi Li, Lu He, and Huijuan Xu. Weakly-supervised temporal action detection for fine-grained videos with hierarchical atomic actions. In *ECCV*, 2022. 2
- [31] Kevin Qinghong Lin, Jinpeng Wang, Mattia Soldan, Michael Wray, Rui Yan, Eric Z Xu, Difei Gao, Rong-Cheng Tu, Wenzhe Zhao, Weijie Kong, et al. Egocentric video-language pretraining. In *NeurIPS*, 2022. 2
- [32] Shaowei Liu, Subarna Tripathi, Somdeb Majumdar, and Xiaolong Wang. Joint hand motion and interaction hotspots prediction from egocentric videos. In *CVPR*, 2022. 2
- [33] Ze Liu, Yutong Lin, Yue Cao, Han Hu, Yixuan Wei, Zheng Zhang, Stephen Lin, and Baining Guo. Swin transformer: Hierarchical vision transformer using shifted windows. In *ICCV*, 2021. 3

- [34] Pascal Mettes, William Thong, and Cees GM Snoek. Object priors for classifying and localizing unseen actions. *IJCV*, 129(6):1954–1971, 2021. 2
- [35] Jungin Park, Jiyoung Lee, and Kwanghoon Sohn. Dual-path adaptation from image to video transformers. In *CVPR*, 2023. 3
- [36] AJ Piergiovanni, Anelia Angelova, and Michael S Ryoo. Differentiable grammars for videos. In *AAAI*, 2020. 2
- [37] Chiara Plizzari, Mirco Planamente, Gabriele Goletto, Marco Cannici, Emanuele Gusso, Matteo Matteucci, and Barbara Caputo. E2 (go) motion: Motion augmented event stream for egocentric action recognition. In *CVPR*, 2022. 4
- [38] Shraman Pramanick, Yale Song, Sayan Nag, Kevin Qinghong Lin, Hardik Shah, Mike Zheng Shou, Rama Chellappa, and Pengchuan Zhang. Egovlpv2: Egocentric video-language pre-training with fusion in the backbone. In *ICCV*, 2023. 2
- [39] Richard Ramsey, David M. Kaplan, and Emily S. Cross. Watch and learn: The cognitive neuroscience of learning from others’ actions. *Trends in Neurosciences*, 44(6):478–491, 2021. 1
- [40] Marcus Rohrbach, Anna Rohrbach, Michaela Regneri, Sikandar Amin, Mykhaylo Andriluka, Manfred Pinkal, and Bernt Schiele. Recognizing fine-grained and composite activities using hand-centric features and script data. *IJCV*, 119:346–373, 2016. 2
- [41] Stefan Schaal. Learning from demonstration. In *NeurIPS*, 1996. 1
- [42] Christoph Schuhmann, Richard Vencu, Romain Beaumont, Robert Kaczmarczyk, Clayton Mullis, Aarush Katta, Theo Coombes, Jenia Jitsev, and Aran Komatsuzaki. Laion-400m: Open dataset of clip-filtered 400 million image-text pairs. In *NeurIPS Workshop*, 2021. 5, 6, 11
- [43] Pierre Sermanet, Corey Lynch, Yevgen Chebotar, Jasmine Hsu, Eric Jang, Stefan Schaal, Sergey Levine, and Google Brain. Time-contrastive networks: Self-supervised learning from video. In *ICRA*, 2018. 5, 6, 7, 13, 14, 15
- [44] Dandan Shan, Jiaqi Geng, Michelle Shu, and David F Fouhey. Understanding human hands in contact at internet scale. In *CVPR*, 2020. 2, 4
- [45] Gunnar A Sigurdsson, Abhinav Gupta, Cordelia Schmid, Ali Farhadi, and Karteek Alahari. Actor and observer: Joint modeling of first and third-person videos. In *CVPR*, 2018. 5, 6, 7, 13, 14, 15
- [46] Gunnar A Sigurdsson, Abhinav Gupta, Cordelia Schmid, Ali Farhadi, and Karteek Alahari. Charades-ego: A large-scale dataset of paired third and first person videos. *arXiv preprint arXiv:1804.09626*, 2018. 5
- [47] Hao Tan, Jie Lei, Thomas Wolf, and Mohit Bansal. Vimpac: Video pre-training via masked token prediction and contrastive learning. *arXiv preprint arXiv:2106.11250*, 2021. 2
- [48] Bugra Tekin, Federica Bogo, and Marc Pollefeys. H+ o: Unified egocentric recognition of 3d hand-object poses and interactions. In *CVPR*, 2019. 2
- [49] Zhan Tong, Yibing Song, Jue Wang, and Limin Wang. VideoMAE: Masked autoencoders are data-efficient learners for self-supervised video pre-training. In *NeurIPS*, 2022. 2, 3
- [50] Huiyu Wang, Mitesh Kumar Singh, and Lorenzo Torresani. Ego-only: Egocentric action detection without exocentric transferring. In *CVPR*, pages 5250–5261, 2023. 3
- [51] Qitong Wang, Long Zhao, Liangzhe Yuan, Ting Liu, and Xi Peng. Learning from semantic alignment between unpaired multiviews for egocentric video recognition. In *ICCV*, 2023. 2
- [52] Rui Wang, Dongdong Chen, Zuxuan Wu, Yinpeng Chen, Xiyang Dai, Mengchen Liu, Lu Yuan, and Yu-Gang Jiang. Masked video distillation: Rethinking masked feature modeling for self-supervised video representation learning. In *CVPR*, 2023. 4
- [53] Chen Wei, Haoqi Fan, Saining Xie, Chao-Yuan Wu, Alan Yuille, and Christoph Feichtenhofer. Masked feature prediction for self-supervised visual pre-training. In *CVPR*, 2022. 2
- [54] Zihui Xue and Kristen Grauman. Learning fine-grained view-invariant representations from unpaired ego-exo videos via temporal alignment. In *NeurIPS*, 2023. 2, 4, 5, 6, 7, 11, 12, 13, 14, 15
- [55] Huangyue Yu, Minjie Cai, Yunfei Liu, and Feng Lu. What i see is what you see: Joint attention learning for first and third person video co-analysis. In *ACMMM*, 2019. 2
- [56] Rowan Zellers and Yejin Choi. Zero-shot activity recognition with verb attribute induction. In *EMNLP*, 2017. 2
- [57] Chuhan Zhang, Ankush Gupta, and Andrew Zisserman. Temporal query networks for fine-grained video understanding. In *CVPR*, 2021. 2
- [58] Weiyu Zhang, Menglong Zhu, and Konstantinos G Derpanis. From actemes to action: A strongly supervised representation for detailed action understanding. In *ICCV*, 2013. 11

Appendix

In this document, we provide more concrete details of the AE2 benchmark [54] in Appendix A, additional experimental results in Appendix B, including the results using different backbones (CLIP pretrained ViT-L/14 [11] and ResNet-50 [20]), few-shot classification and frame retrieval performance, ablation studies for each hyper-parameter, and analysis for the failure case. Finally, we present the broader impact of our **BYOV** in Appendix C.

A. Benchmark Details

In this section, we provide a detailed explanation of AE2 benchmark [54] and the evaluation details of four downstream tasks, including action phase classification, frame retrieval, phase progression, and Kendall’s τ .

A.1. Datasets

The AE2 benchmark [54] contains four datasets: (1) Break Eggs; (2) Pour Mild; (3) Pour Liquid; and (4) Tennis Forehand. The summary of each dataset is shown in Tab. A1.

- **Break Eggs** sampled from the CMU-MMAC dataset [28] contains 5 different cooking recipes (brownies, pizza, sandwiches, salad, and scrambled eggs) captured by 43 users. While the ego and exo videos are strictly synchronized (i.e., capturing the same scene), we do not use the correspondence between videos for training.
- **Pour Milk** sampled from the H2O dataset [27] contains the scene of 10 users interacting with a milk carton using their hands. The dataset provides one egocentric video and four exocentric static videos for each scene. Some ego and exo video pairs are synchronized and the rest are asynchronous.
- **Pour Liquid** assumes a more challenging scenario as the ego and exo videos are sampled from different datasets. Therefore, those videos are fully asynchronous and captured from different environments. The ego videos consist of the “pour water” class in EPIC-Kitchens [8] and the exo videos are the “pour” category in HMDB51 [26].
- **Tennis Forehand** includes outdoor activity videos. The exocentric videos of the tennis forehand action are sampled from the Penn Action [58] dataset and the egocentric videos are collected from 12 players using the Go Pro HERO8 camera. The videos are asynchronous, covering real-world scenarios.

A.2. Downstream tasks

- **Action phase classification** aims to predict an atomic action phase label corresponding to a given frame. The Break Eggs dataset contains four action phases between ‘start’, ‘hit egg’, ‘visible crack on the eggshell’, ‘egg contents released’, and ‘end.’ The Pour Milk and Pour Liquid datasets contain three phases between ‘start’, ‘liquid

exits container’, ‘pouring complete’, and ‘end.’ The Tennis Forehand dataset has only two phases between ‘start’, ‘racket touches ball’, and ‘end.’ In this document, we additionally provide a few-shot classification performance to validate the robustness of **BYOV**.

- **Frame retrieval** selects frames corresponding to a given frame using the NN search. We evaluate this task with mean average precision (mAP)@K (K=5,10,15) in the regular and cross-view settings.
- **Phase progression** quantifies how effectively the learned representations imply the progression of an action. The progression value within each phase is defined as the normalized temporal difference between the timestamp of a given frame and those of key events, scaled by the total number of frames in the video. A linear regressor is then employed to predict the phase progression values from the embeddings, where our encoders are frozen. The performance is evaluated using the average R -squared value as follows:

$$R^2 = 1 - \frac{\sum_{t=1}^T (y_t - \hat{y}_t)^2}{\sum_{t=1}^T (y_t - \bar{y})^2},$$

where y_t is the ground truth phase progress value, \bar{y} is the average value of all y_t , and \hat{y}_t is the prediction from the linear regressor. The maximum value of R^2 is 1.

- **Kendall’s τ** assesses the temporal alignment between two sequences by comparing the order of frames. Specifically, we first sample a pair of frames from one video, (u_i, u_j) , and retrieve their nearest corresponding frames in the other video, (v_p, v_q) . A set of frame indices (i, j, p, q) is treated as ‘matched’ if the temporal order of u_i and u_j and that of v_p and v_q are the same. Kendall’s τ is then computed by,

$$\tau = \frac{\# \text{matched pairs} - \# \text{not matched pairs}}{\# \text{all possible pairs}}.$$

A value of 1 means the frame representations are perfectly aligned while -1 indicates the representations are aligned in the reverse order.

B. Additional Experiments

B.1. Results with different frame encoders

We mainly used the CLIP pretrained ViT-B/16 [11] to encode each frame in the main paper. To demonstrate the robustness of **BYOV** according to the frame encoders, we train **BYOV** with the CLIP pretrained ViT-L/14 [11] and ResNet-50 [20], and evaluate the performance on four tasks for four datasets. Implementation details for each frame encoder are as follows.

- **CLIP ViT-L/14** [11] pretrained on LAION-400M [42] projects each frame into 1024-dimensional 256 token embeddings different from the ViT-B/16, which has 768-dimensional 196 token embeddings. We keep the number

Table A1. Performance with respect to variants of the components in **BYOV**. We report the performance evaluated on the Break Eggs dataset.

Dataset	# Train		# Val		# Test		Fixed exo-view	Sync. ego-exo
	Ego	Exo	Ego	Exo	Ego	Exo		
(A) Break Eggs	61	57	5	5	10	10	✓	✓
(B) Pour Milk	29	48	4	8	7	16	✓	✗
(C) Pour Liquid	70	67	10	9	19	18	✗	✗
(D) Tennis Forehand	94	79	25	24	50	50	✗	✗

Table A2. Performance comparison with various frame encoders on the AE2 benchmark [54]. The benchmark consists of four sub-tasks: (A) Break Eggs, (B) Pour Milk, (C) Pour Liquid, and (D) Tennis Forehand. The top results are highlighted in **bold** and the second-best results are underlined.

Task	Method	Classification (F1 score)			Frame Retrieval (mAP@10)			Phase progression	Kendall's τ
		Regular	Ego2Exo	Exo2Ego	Regular	Ego2Exo	Exo2Ego		
(A)	Random features	19.18	18.93	19.45	47.13	41.74	37.19	-0.0572	0.0018
	ImageNet features	50.24	21.48	32.25	50.49	33.09	37.80	-0.1446	0.0188
	CLIP ViT-B/16	51.66	27.97	26.24	44.46	35.85	35.70	0.0402	0.0168
	CLIP ViT-L/14	54.24	41.56	38.31	38.14	38.96	34.99	0.1672	0.0483
	AE2 [54]	66.23	57.41	<u>71.72</u>	65.85	64.59	62.15	0.5109	0.6316
	BYOV (ResNet-50)	<u>72.57</u>	67.91	70.74	<u>68.42</u>	63.27	63.85	0.7751	0.7463
	BYOV (ViT-B/16)	74.30	75.01	71.28	67.17	70.65	69.02	0.8533	0.9451
	BYOV (ViT-L/14)	72.41	<u>70.11</u>	72.92	75.59	<u>67.73</u>	<u>67.55</u>	<u>0.8272</u>	<u>0.8940</u>
	(B)	Random features	36.84	33.96	41.97	52.48	50.56	51.98	-0.0477
ImageNet features		41.59	39.93	45.52	54.09	27.31	43.21	-2.6681	0.0115
CLIP ViT-B/16		43.24	49.21	30.94	52.16	46.39	40.34	-4.0754	0.0046
CLIP ViT-L/14		46.65	46.79	17.77	46.20	44.32	53.75	-0.4735	0.0503
AE2 [54]		85.17	84.73	82.77	84.90	78.48	<u>83.41</u>	0.7634	0.9062
BYOV (ResNet-50)		86.84	83.83	87.00	87.17	79.27	79.87	0.8082	0.9152
BYOV (ViT-B/16)		86.46	<u>85.09</u>	<u>86.61</u>	89.42	87.73	85.06	0.8992	0.9466
BYOV (ViT-L/14)		<u>86.76</u>	85.54	86.58	<u>87.35</u>	<u>82.51</u>	82.61	<u>0.8407</u>	<u>0.9448</u>
(C)		Random features	45.26	47.45	44.33	49.83	55.44	55.75	-0.1303
	ImageNet features	53.13	22.44	44.61	51.49	52.17	30.44	-1.6329	-0.0053
	CLIP ViT-B/16	60.60	36.97	48.43	43.63	47.58	37.02	-0.3139	-0.0048
	CLIP ViT-L/14	54.38	6.83	51.69	50.01	31.82	54.61	-0.2066	-0.0052
	AE2 [54]	66.56	57.15	65.60	65.54	65.79	57.35	0.1380	0.0934
	BYOV (ResNet-50)	78.63	73.67	<u>76.53</u>	71.47	66.74	<u>71.17</u>	0.3982	0.2883
	BYOV (ViT-B/16)	79.48	<u>71.83</u>	76.23	<u>71.06</u>	<u>75.03</u>	70.03	<u>0.4483</u>	<u>0.3052</u>
	BYOV (ViT-L/14)	79.48	71.49	76.61	70.36	76.48	73.38	0.4534	0.3084
	(D)	Random Features	30.31	33.42	28.10	66.47	58.98	59.87	-0.0425
ImageNet Features		69.15	42.03	58.61	76.96	66.90	60.31	-0.4143	0.0734
CLIP ViT-B/16		67.81	43.41	44.22	74.54	59.57	52.02	-0.4996	0.0618
CLIP ViT-L/14		64.40	47.53	47.50	74.26	67.19	58.73	-0.4126	0.0302
AE2 [54]		85.87	84.71	85.68	86.83	81.46	82.07	0.5060	0.6171
BYOV (ResNet-50)		<u>89.34</u>	94.83	84.96	89.83	86.71	82.68	0.7588	0.7599
BYOV (ViT-B/16)		89.12	94.47	<u>85.73</u>	<u>90.61</u>	88.34	88.94	0.7881	<u>0.7852</u>
BYOV (ViT-L/14)		89.56	<u>94.48</u>	86.51	91.21	<u>87.04</u>	<u>88.33</u>	<u>0.7653</u>	0.8101

of layers of the encoder $g_\phi(\cdot)$ and the decoder $h_\psi(\cdot)$ as 12 and 4 while setting the size of the latent space to 512. The

number of trainable parameters is 51.8M (38.4M for the encoder and 13.4M for the decoder, respectively). The to-

Table A3. Performance comparison for few-shot classification and regular frame retrieval on the AE2 benchmark [54]. The benchmark consists of four sub-tasks: (A) Break Eggs, (B) Pour Milk, (C) Pour Liquid, and (D) Tennis Forehand. We report the few-shot classification (F1 score) and regular frame retrieval (mAP@5, mAP@10, and mAP@15) performance. The top results are highlighted in **bold** and the second-best results are underlined.

Task	Method	Few-shot Classification (F1 score)			Regular Frame Retrieval		
		10%	50%	100%	mAP@5	mAP@10	mAP@15
(A)	Random features	19.18	19.18	19.18	48.26	47.13	45.75
	ImageNet features	46.15	48.80	50.24	49.98	50.49	50.08
	CLIP ViT-B/16	46.46	49.18	51.66	44.89	44.46	43.44
	CLIP ViT-L/14	47.36	51.80	54.24	38.47	38.14	37.72
	ActorObserverNet [45]	31.40	35.63	36.14	50.92	50.47	49.72
	TCN [43] (single-view)	52.30	54.90	56.90	52.82	53.42	53.60
	TCN [43] (multi-view)	56.88	59.25	59.91	59.11	58.83	58.44
	TCN [43] (unpaired multi-view)	56.13	56.65	56.79	58.18	57.78	57.21
	CARL [4]	39.18	41.92	43.43	47.14	46.04	44.99
	TCC [13]	57.54	59.18	59.84	59.33	58.75	57.99
	GTA [19]	56.89	56.77	56.86	62.79	61.55	60.38
	AE2 [54]	<u>63.95</u>	<u>64.86</u>	<u>66.23</u>	<u>66.86</u>	<u>65.85</u>	<u>64.73</u>
	BYOV (ViT-B/16)	71.84	73.92	74.30	67.28	67.17	66.40
	(B)	Random features	36.84	33.96	41.97	52.48	50.56
ImageNet features		41.59	39.93	45.52	54.09	27.31	43.21
CLIP ViT-B/16		39.44	38.90	43.24	53.29	52.16	51.55
CLIP ViT-L/14		42.68	39.91	46.65	46.20	46.20	53.75
TCN [43] (single-view)		43.60	46.83	47.39	56.98	57.00	56.46
CARL [4]		48.73	48.78	48.79	55.29	55.01	54.23
TCC [13]		78.69	77.97	77.91	81.22	80.97	80.46
GTA [19]		79.82	80.96	81.11	80.65	80.12	79.68
AE2 [54]		<u>85.17</u>	<u>85.12</u>	<u>85.17</u>	<u>85.25</u>	<u>84.90</u>	<u>84.55</u>
BYOV (ViT-B/16)		86.12	86.44	86.46	90.99	89.42	88.98
(C)	Random features	45.26	47.45	44.33	49.83	55.44	55.75
	ImageNet features	53.13	22.44	44.61	51.49	52.17	30.44
	CLIP ViT-B/16	57.21	35.46	60.60	42.34	43.63	44.03
	CLIP ViT-L/14	51.72	28.30	54.38	48.56	50.01	50.52
	TCN [43] (single-view)	54.62	55.08	54.02	48.50	48.83	49.03
	CARL [4]	51.68	55.67	56.98	55.03	55.29	54.93
	TCC [13]	52.37	51.70	52.53	62.93	62.33	61.44
	GTA [19]	55.91	56.87	56.92	62.83	62.79	62.12
	AE2 [54]	<u>65.88</u>	<u>66.53</u>	<u>66.56</u>	<u>66.55</u>	<u>65.54</u>	<u>64.66</u>
	BYOV (ViT-B/16)	79.10	79.28	79.48	73.89	71.06	67.83
(D)	Random Features	30.31	33.42	28.10	66.47	58.98	59.87
	ImageNet Features	69.15	42.03	58.61	76.96	66.90	60.31
	CLIP ViT-B/16	70.37	48.01	67.81	76.45	74.54	73.15
	CLIP ViT-L/14	68.44	42.95	64.40	75.61	74.26	73.14
	TCN [43] (single-view)	65.78	69.19	68.87	74.05	73.76	73.10
	CARL [4]	58.89	59.38	59.69	72.94	69.43	67.14
	TCC [13]	67.71	77.07	78.41	82.78	80.24	78.59
	GTA [19]	80.31	83.04	83.63	86.59	85.20	84.33
	AE2 [54]	<u>85.24</u>	<u>85.72</u>	<u>85.87</u>	<u>87.94</u>	<u>86.83</u>	<u>86.05</u>
	BYOV (ViT-B/16)	88.78	89.01	89.12	90.89	90.61	90.87

Table A4. Performance comparison for cross-view retrieval on the AE2 benchmark [54]. The benchmark consists of four sub-tasks: (A) Break Eggs, (B) Pour Milk, (C) Pour Liquid, and (D) Tennis Forehand. We report the cross-view frame retrieval (mAP@5, mAP@10, and mAP@15) performance. The top results are highlighted in **bold** and the second-best results are underlined.

Task	Method	Ego2Exo Frame Retrieval			Exo2Ego Frame Retrieval		
		mAP@5	mAP@10	mAP@15	mAP@5	mAP@10	mAP@15
(A)	Random features	42.51	41.74	40.51	38.08	38.19	37.10
	ImageNet features	33.32	33.09	32.78	38.99	37.80	36.71
	CLIP ViT-B/16	35.80	35.85	34.92	34.91	35.70	35.96
	CLIP ViT-L/14	39.30	38.94	38.14	35.23	34.99	33.98
	ActorObserverNet [45]	43.57	42.70	41.56	42.00	41.29	40.48
	TCN [43] (single-view)	31.12	32.63	33.73	34.67	34.91	35.31
	TCN [43] (multi-view)	46.38	47.04	46.96	52.50	52.68	52.43
	TCN [43] (unpaired multi-view)	55.34	54.64	53.75	58.79	57.87	57.07
	CARL [4]	37.89	37.38	36.57	40.37	39.94	39.38
	TCC [13]	62.11	61.11	60.33	62.39	62.03	61.25
	GTA [19]	57.11	56.25	55.10	54.47	53.93	53.22
	AE2 [54]	<u>65.70</u>	<u>64.59</u>	<u>63.76</u>	<u>62.48</u>	<u>62.15</u>	<u>61.80</u>
	BYOV (ViT-B/16)	72.76	70.65	70.27	71.79	69.02	68.94
(B)	Random features	51.46	50.56	48.93	52.78	51.98	50.82
	ImageNet features	25.72	27.31	28.57	41.50	43.21	43.06
	CLIP ViT-B/16	46.37	46.39	46.86	41.28	40.34	39.86
	CLIP ViT-L/14	43.71	44.32	44.20	55.55	53.75	53.10
	TCN [43] (single-view)	47.00	46.48	45.42	47.94	47.20	46.59
	CARL [4]	54.35	52.99	51.99	51.14	51.51	51.00
	TCC [13]	75.54	75.30	75.02	80.44	80.27	80.18
	GTA [19]	72.55	72.78	72.96	75.16	75.40	75.48
	AE2 [54]	<u>78.21</u>	<u>78.48</u>	<u>78.78</u>	<u>83.88</u>	<u>83.41</u>	<u>83.05</u>
	BYOV (ViT-B/16)	85.15	87.73	87.80	85.48	85.06	85.00
(C)	Random features	55.78	55.44	54.77	56.31	55.75	54.56
	ImageNet features	51.44	52.17	52.38	30.18	30.44	30.40
	CLIP ViT-B/16	42.08	47.58	49.78	35.14	37.02	36.71
	CLIP ViT-L/14	32.33	31.82	31.59	54.01	54.61	54.64
	TCN [43] (single-view)	53.60	55.28	55.46	29.16	31.15	31.95
	CARL [4]	59.59	59.37	59.19	34.73	36.80	38.10
	TCC [13]	55.98	56.08	56.13	<u>58.11</u>	<u>57.89</u>	<u>57.15</u>
	GTA [19]	57.03	58.52	59.00	51.71	53.32	53.54
	AE2 [54]	<u>66.23</u>	<u>65.79</u>	<u>65.00</u>	57.42	57.35	57.03
	BYOV (ViT-B/16)	79.06	75.03	72.73	76.21	70.03	69.44
(D)	Random Features	61.24	58.98	56.94	63.42	59.87	57.57
	ImageNet Features	69.34	66.90	64.95	61.61	60.31	58.55
	CLIP ViT-B/16	60.63	59.57	58.46	52.25	52.02	52.12
	CLIP ViT-L/14	69.02	67.19	65.44	61.83	58.73	57.05
	TCN [43] (single-view)	54.12	55.08	55.05	56.70	56.65	55.84
	CARL [4]	52.18	54.83	55.39	65.94	63.19	60.83
	TCC [13]	57.87	55.84	53.81	48.62	47.27	46.11
	GTA [19]	78.93	78.00	77.01	79.95	79.14	78.52
	AE2 [54]	<u>82.58</u>	<u>81.46</u>	<u>80.75</u>	<u>82.82</u>	<u>82.07</u>	<u>81.69</u>
	BYOV (ViT-B/16)	88.55	88.34	87.98	90.64	88.94	87.26

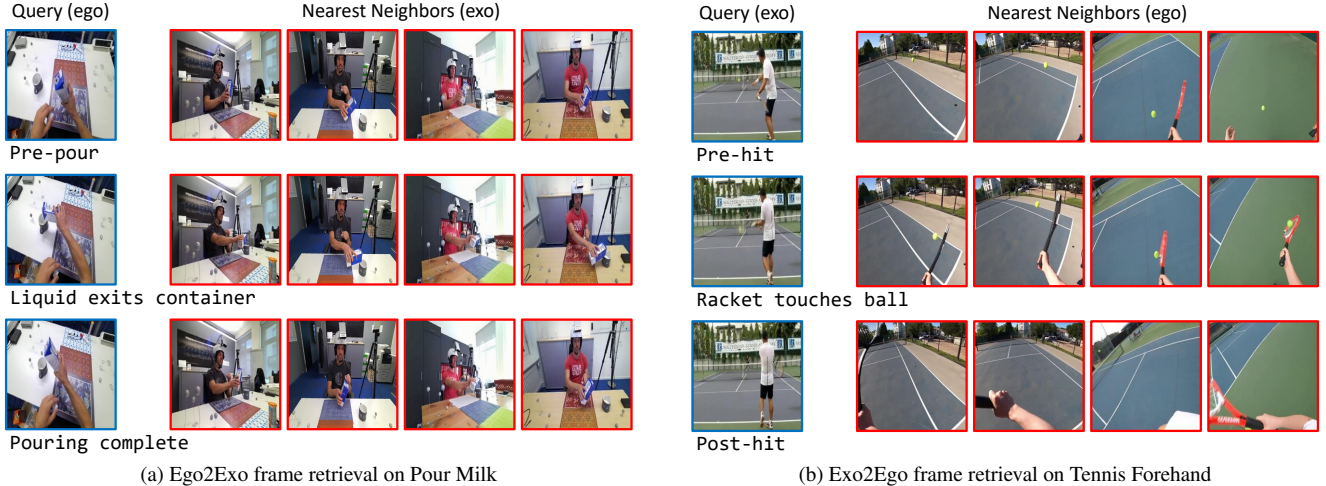


Figure A1. Qualitative examples of frame retrieval from the Pour Milk and Tennis Forehand datasets. We retrieve the nearest neighbor frames (red box) corresponding to the given query frame (blue box).

Table A5. Performance comparison according to various sizes of latent space in **BYOV**. We evaluate the performance on the Break Eggs dataset.

Latent Size	Trainable Params	Classification (F1 score)			Frame Retrieval (mAP@10)			Phase progression	Kendall's τ
		Regular	Ego2Exo	Exo2Ego	Regular	Ego2Exo	Exo2Ego		
64	0.9M	<u>71.55</u>	71.34	69.36	65.87	64.09	68.16	0.8362	0.8943
128	3.4M	70.84	<u>72.74</u>	<u>69.71</u>	67.07	66.70	68.45	<u>0.8407</u>	<u>0.9240</u>
256	12.3M	74.30	75.01	71.28	<u>67.17</u>	<u>70.65</u>	<u>69.02</u>	0.8533	0.9451
512	51.5M	70.89	70.19	68.72	68.70	73.29	74.45	0.8107	<u>0.9240</u>

ken selection ratio in selective token merging (STM), and the masking ratio in masked self-view modeling (MSM) and masked cross-view modeling (MCM) are set to 0.3, 0.4, and 0.8 as with the ViT-B/16.

- **ResNet-50** [20] employs convolutional neural network, and is pretrained on ImageNet-1K [9]. We extract the feature for each frame from a *Conv4c* layer of ResNet-50, which has 14×14 resolution with 1024 dimensions. We also perform the selective token merging to keep the overall framework of **BYOV**. The receptive field of each 1024-d embedding is 55×55 pixels, which is wider than 16×16 in ViT-B/16. Therefore, we reduce the selection ratio to 0.1. The masking ratio in MSM and MCM are set to 0.4 and 0.8, respectively. Similar to the ViT-L/14, we use 512-dimensional latent space for the encoder $g_\phi(\cdot)$ and the decoder $h_\psi(\cdot)$.

In Tab. A2, we first provide the zero-shot performance of the ResNet-50 (ImageNet features), CLIP ViT-B/16, and CLIP ViT-L/14. While ViT-L/14 (303M) has about three times more parameters than ViT-B/16 (86M), comparisons between the two frame encoders show that generalization capability is not dependent on the model size. Meanwhile, our **BYOV** with various frame encoders consistently out-

performs the state-of-the-art [54] across tasks and datasets. In practice, **BYOV** with the ResNet-50 surpasses AE2 [54] without any additional information such as bounding boxes from the hand-object detector as in [54]. It demonstrates the robustness of the framework of our **BYOV**.

B.2. Few-shot classification

Following [54], we compare few-shot classification performance with the state-of-the-art methods [4, 13, 19, 43, 45, 54] in Tab. A3. We train the SVM classifier using 10% (or 50%) of the latents from the training data and evaluate the classification performance. Note that we train **BYOV** ten times on non-overlapped few-shot training data and report the average performance. Tab. A3 demonstrates the superior performance of **BYOV**, showing significant performance gaps to the existing works across all datasets. In particular, **BYOV** trained with only 10% training data significantly outperforms the prior best performance [54] trained with 100% training data by a large margin of 12.54 on the Pour Liquid dataset.

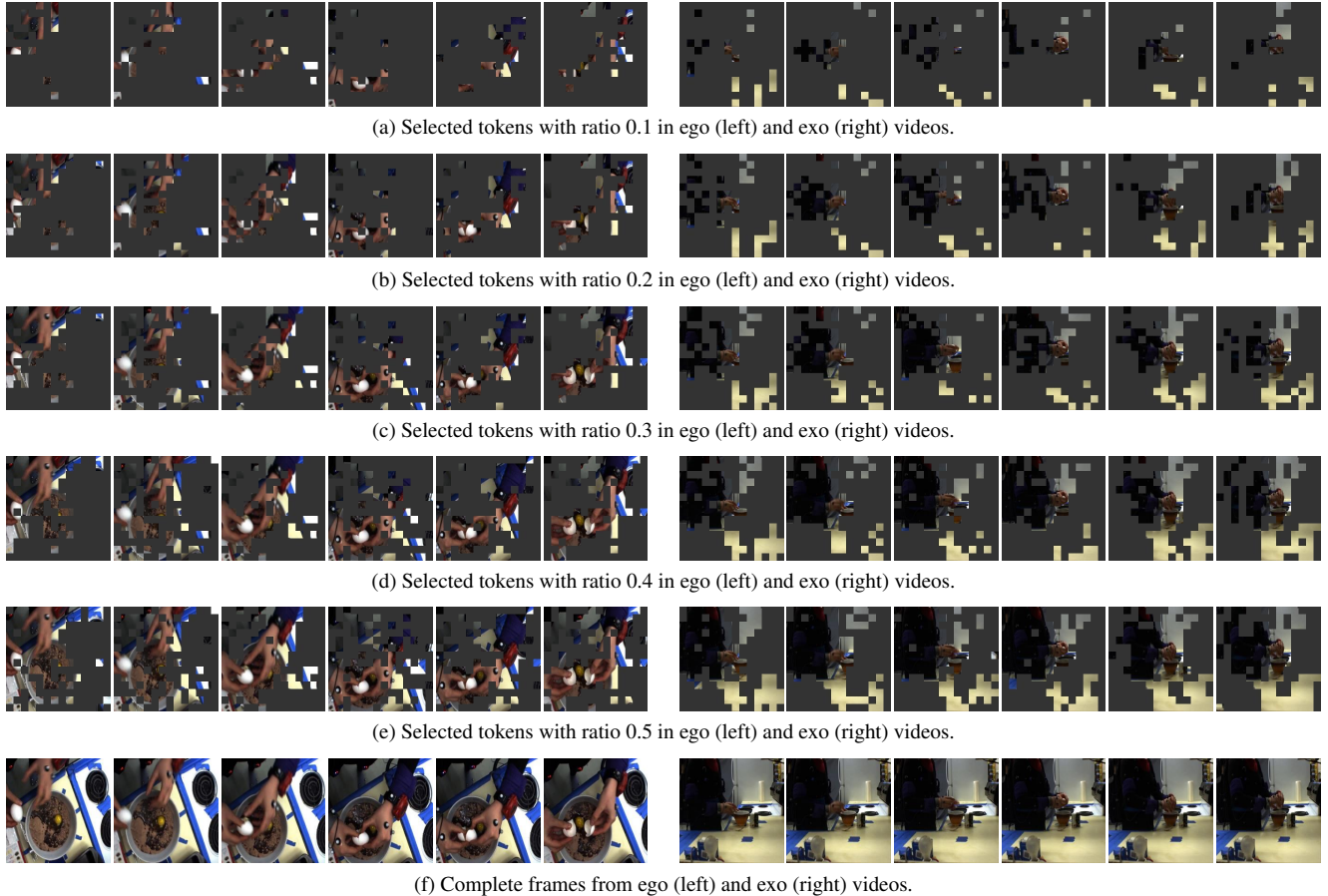


Figure A2. Visualization of selected tokens at each frame sampled from ego (left) and exo (right) videos. Note that complete frames are identical with the token selection ratio of 1.0.

B.3. Frame retrieval

In Tab. A3 and Tab. A4, we report the frame retrieval performance, evaluated in both regular and cross-view settings. Comparisons with the existing methods consistently demonstrate the effectiveness of **BYOV** in both regular and cross-view retrieval across all datasets, showing an average performance improvement of about 10%.

We illustrate examples of cross-view frame retrieval from the Pour Milk and Tennis Forehand datasets in Fig. A1. Given the query frame (blue box) from one view, we retrieve the frames (red box) from the other view videos using NN search. The results show that the query and retrieved frames are contextually well-aligned through the action states. In addition, properly retrieved frames demonstrate that **BYOV** captures contexts over time. For example, the frames with the action phases of ‘pre-pour’ and ‘pouring complete’ are visually similar, however, **BYOV** successfully performs frame retrieval by capturing the context with respect to the action state over time. In this regard, we further analyze the effectiveness of **BYOV** by visualizing the frame

embeddings in the following section.

B.4. Ablation study

We analyze the effectiveness of each component in **BYOV**, including the size of latent space, token selection ratio in STM, and masking ratio in MSM and MCM. Note that we use the CLIP pretrained ViT-B/16 as the frame encoder for the following experiments.

Hidden dimension of autoencoders. The encoder $g_\phi(\cdot)$ maps the frame token embeddings into the 256-dimensional latents, such that the encoder and decoder have 9.7M and 2.6M trainable parameters, respectively. To assess the impact of latent space size on performance, we train **BYOV** with various latent sizes and evaluate the performance on the Break Eggs dataset. Tab. A5 summarizes the results, including the performance on downstream tasks and the number of trainable parameters corresponding to each latent size. Naturally, large latent spaces enhance representation capability but lead to more trainable parameters (e.g. 51.5M parameters with a 512-dimensional latent space for 12 encoder and 4 decoder layers) and require more exten-

Table A6. Performance comparison according to variants of the hyperparameters in **BYOV**. We report the performance evaluated on the Break Eggs dataset.

Ratio (%)			Classification (F1 score)			Frame Retrieval (mAP@10)			Phase	Kendall's
STM	MSM	MCM	Regular	Ego2Exo	Exo2Ego	Regular	Ego2Exo	Exo2Ego	progression	τ
<i>Effectiveness of token selection ratio</i>										
10	40	80	41.45	21.13	20.03	56.05	46.06	46.85	0.1858	0.0157
20	40	80	70.97	69.60	66.27	65.05	71.13	64.52	0.6597	0.7978
30	40	80	74.30	75.01	71.28	67.17	70.65	69.02	0.8533	0.9451
40	40	80	<u>72.39</u>	<u>72.59</u>	<u>69.19</u>	68.20	73.79	67.44	<u>0.8299</u>	<u>0.8963</u>
50	40	80	71.56	69.05	68.79	68.20	<u>72.79</u>	67.20	<u>0.8299</u>	0.8926
100	40	80	71.34	72.58	65.07	<u>67.44</u>	69.32	<u>67.87</u>	0.7894	0.8957
<i>Effectiveness of masking ratio in MSM</i>										
30	10	80	70.71	69.51	66.20	67.67	66.10	63.89	0.5228	0.6724
30	20	80	71.22	70.38	69.81	67.67	68.27	65.83	0.8134	0.9126
30	30	80	72.28	73.21	70.22	67.28	70.21	68.15	0.8330	0.9337
30	40	80	74.30	75.01	71.28	<u>67.17</u>	<u>70.65</u>	<u>69.02</u>	0.8533	0.9451
30	50	80	<u>72.87</u>	<u>73.71</u>	<u>70.87</u>	67.28	71.21	70.15	<u>0.8398</u>	<u>0.9410</u>
30	100	80	66.65	69.97	68.24	65.01	67.48	66.86	0.6916	0.7818
<i>Effectiveness of masking ratio in MCM</i>										
30	40	0	67.23	66.65	67.10	60.38	58.44	56.97	0.7019	0.8040
30	40	20	71.40	69.06	70.19	64.98	62.09	61.27	0.8269	0.9112
30	40	40	73.23	73.81	71.17	68.84	65.94	68.22	0.8133	0.9247
30	40	60	<u>73.33</u>	<u>74.54</u>	71.32	<u>67.21</u>	70.65	69.02	<u>0.8480</u>	<u>0.9440</u>
30	40	80	74.30	75.01	<u>71.28</u>	67.17	70.65	69.02	0.8533	0.9451
30	40	100	71.09	70.01	70.47	65.34	<u>66.50</u>	<u>68.63</u>	0.7435	0.8354

sive training data. The results indicate that increasing the latent size from 64 to 256 consistently improves performance. However, a further increase to a 512-dimensional latent space leads to performance degradation, attributed to the limited availability of training data.

Token selection ratio. Selective token merging (STM) allows **BYOV** to effectively capture action-related regions while excluding noisy regions without any training as shown in the main paper. We provide the performance of **BYOV** with various token selection ratios in the first panel of Tab. A6 and depict the selected tokens corresponding to each selection ratio in Fig. A2. The results show that the token selection ratio significantly affects the performance due to the difference in the field of view between ego and exo videos. In other words, a low selection ratio is insufficient to cover the action-related regions in ego videos (see Fig. A2a and Fig. A2b), while a high selection ratio makes noisy tokens be included in exo videos (see Fig. A2e). To balance the lack of information in the ego video and the unnecessary noise in the exo video, we set the token selection ratio to 0.3.

Masking ratio. We validate the effectiveness of the masking ratio in masked self-view modeling (MSM) and masked cross-view modeling (MCM) in the second and third panels of Tab. A6. In MSM, we can guess a low masking ratio enables the model to easily solve each masked model-

ing problem, leading to insufficient causality learning. In practice, the results show significant performance drops in phase progression and Kendall's τ . An extremely high masking ratio in MSM makes learning the causality between frames hard as the decoder takes only a few clean tokens (or only masked tokens with a 100% masking ratio). The low masking ratio in MCM degrades performance for a similar reason as in MSM. Meanwhile, a high masking ratio in MCM makes the masked cross-view modeling significantly difficult to solve with limited training data, showing performance drops across all downstream tasks. **BYOV** trained with the masking ratio of 0.4 and 0.8 in MSM and MCM achieves to produce the effective fine-grained view-invariant video representations.

B.5. Failure cases

While our **BYOV** significantly improves the performance across various benchmarks and experimental protocols, we observed that most failure cases occur in videos with slow movement transitions, particularly in exocentric videos. In such cases, frame embeddings tend to attend to each other uniformly, reducing the model's ability to capture meaningful temporal dependencies. Fig. A3 illustrates a visualization of the softmax similarity score between the final frame embeddings for a failure case from the *Pour Liquid* benchmark. Despite introducing positional embeddings and se-



Figure A3. Visualization of the softmax similarity between final frame embeddings for a failure case from the *Pour Liquid* benchmark. We depict the similarity score between only one reference token embedding (red box) and other token embeddings (blue boxes) for visibility.

lective token merging, the embedding feature for a reference frame (red box) attends to all other embeddings similarly, resulting in less informative final representations. Beyond simple token selection of **BYOV**, learning-based token selection approach [6] may further improve the robustness of learned representations.

C. Broader Impact

By achieving robust, view-invariant learning from unpaired ego-exo videos, **BYOV** can significantly advance the ability of AI to understand human actions and interactions across diverse perspectives, contributing to a wide range of real-world applications such as robotics, augmented and virtual reality, and assistive technologies. Moreover, this research can facilitate new related research as follows;

- **Cross-view video generation:** The video representations learned by **BYOV** contain fine-grained action context. In addition, the decoders used during training show a high recovery rate. This shows that it is possible to generate videos across views, which can be used to generate educational or instructional videos.
- **Multi-view activity tracking:** The view-consistent representations can be used in continuously tracking a person or object across various camera views (ego and exo) to maintain consistent identity and action recognition across perspectives, useful for applications in security and autonomous vehicles.